VOLUME 237 (11) JUNE 2007 ISSN 0029-5493

Nuclear Engineering and Design

An International Journal devoted to all aspects of Nuclear Fission Energy

CONTENTS

Engineering Mechanics
Modeling approaches for strongly non-homogeneous two-phase flows
C. Morel 1107
Seismic proof test of a reinforced concrete containment vessel (RCCV). Part 3. Evaluation of seismic safety margin
T. Hirama, M. Goto, H. Kumagai, Y. Naito, A. Suzuki, H. Abe, K. Takiguchi and H. Akiyama 1128

Reactor Components
Corrosion-induced bond strength degradation in reinforced concrete—Analytical and empirical models
K. Bhargava, A.K. Ghosh, Y. Mori and S. Ramanujam 1140

Core Physic
Pu-breeding feasibility in PWR
J.F.A. Delbeke, G. Janssens-Maenhout and P. Peerani 1158

Thermal Hydraulics
On the analogies in the dynamic behaviour of heated channels with boiling and supercritical fluids
W. Ambrosini 1164
A numerical investigation of three-dimensional flows in large volumes in the context of passive containment cooling in BWRs
B.L. Smith 1175

Safety and Risk Analysis
A web-based nuclear simulator using RELAP5 and LabVIEW
K.D. Kim and Rizwan-uddin 1185

Experiments
Analysis of the Leibstadt power plant condensate and feedwater systems during selected operational transients
O. Zerkak, P. Coddington and H. Eitschberger 1195

Waste Management
Feasibility study of a microsystem to analyse radioactive solutions
G. Janssens-Maenhout and S. Nucifora 1209
Instructions to Contributors I

Available online at ScienceDirect www.sciencedirect.com

Affiliated with the European Nuclear Society (ENS) and with the International Association for Structural Mechanics in Reactor Technology, e.V. (IASMiRT)

Available online at www.sciencedirect.com
ScienceDirect
Nuclear Engineering and Design 237 (2007) 1209–1219
Nuclear Engineering and Design
www.elsevier.com/locate/nucengdes

Feasibility study of a microsystem to analyse radioactive solutions

G. Janssens-Maenhout [a,b,*], S. Nucifora [b,c]

[a] *Joint Research Centre Ispra, IPSC – Nuc. Saf./Trac. Vuln., Via Fermi, 1 T.P. 361, I-21020 ISPRA, Italy*
[b] *University Ghent, Engineering Faculty TW08, Techn. park Zwijnaerde B914, B-9051 Ghent, Belgium*
[c] *Joint Research Centre Karlsruhe, ITU – Nuc. Chem., Postfach 2340, D-76125 Karlsruhe, Germany*

Received 11 October 2006; received in revised form 1 December 2006; accepted 14 December 2006

Abstract

The application of micro-electro-mechanical systems (MEMS) to evaluate the chemical properties of radioactive solutions has been investigated with the example of a liquid sample taken from reprocessing plant vessels. For radiochemical solutions the application of a microvial instead of a millivial bears more advantages than for other chemical solutions because of the strongly simplified sample preparation and significantly reduced dose uptake. The scaling down of the liquid sample might also cause negative implications on the radiochemical analyses with regard to accuracy and representativeness. All the consequences on replacing a liquid sample of several millilitres by one of less than 1 μl are investigated. This paper reports in particular on a first feasibility study of the replacement of a millivial by a microvial for the analysis of spent fuel solutions in a reprocessing plant for the purpose of nuclear safeguards. Implementation of MEMS in this area results in a reduction in dose that is almost proportional with the reduction in size. This brings about a simplification in sample preparation and a significant reduction in dose uptake for the analyst with many advantages over conventional methods. The MEMS designed for analyzing a spent fuel solution consists of three microchannels: one channel for the sample, one for a reference solution, and one is the blank.

The concentration of the solution is determined by the photospectra of the light transmitted along the channel axis and absorbed at nuclide-specific wavelengths. Absorptiometry experiments with a micro-volume demonstrated the validity of the Beer–Lambert law and derived the limits in precision as a function of the concentration. A photospectrometric database for the reference solution of aqueous solutions of nitric acid with the neodymium surrogate was setup.

Electrophoretic forces fill the subject microchannel with the solution, which will release heat due to radioactive decay. The flow and heat characteristics of microchannels have been observed to deviate from conventional and well established theory. These differences have been evaluated and the reasons examined. The microscopic effect of the electrical double layer (EDL) is focused on. These investigations on the validity of the traditional macroscopic models allowed application of classical theories within a well defined validity range and the adaptation of these theories to suit microscopic models. It was concluded that for acid solutions the EDL can be neglected. With thermodynamic simulations the stresses were evaluated. Conditions on the released heat were derived that guarantee no deformation of the chip and no temperature shift for the absorptiometry measurements.

1. Introduction

Significant progress in microfabrication techniques enables the manufacturing of today's microsystems, with a large and steadily growing application potential in the area of micro-electronics, analytical chemistry, pharmaceutics, and bio-chemistry. These "systems on a microchip" are realised by integrating on a substrate mechanical actuators, sensors and (opto-)electronics, all devices with the size of 1 μm to 1 mm.

The starting key element is the micro-electro-mechanical system (MEMS) as actuator, which is a sophisticated functional, fluid manipulating device on a small silicon chip, produced at low costs. A cheap mass production of miniaturised single-use analysis microchips is possible by the hot embossing technique.

Since microsystems proved to be very efficient, economic and performant to analyse chemical solutions in microvials, it was investigated if these microsystems could be introduced to analyse radioactive solutions in the nuclear reprocessing industry. Applications are numerous: for safeguards reasons it is needed to accurately determine the total content U and Pu in the input and output accountancy tanks, for which several millilitres of solution are taken to undergo concentration measurements. In a first

* Corresponding author.
E-mail address: greet.maenhout@jrc.it (G. Janssens-Maenhout).

0029-5493/$ – see front matter © 2007 Elsevier B.V. All rights reserved.
doi:10.1016/j.nucengdes.2006.12.005

Nomenclature

a	half microchannel width (m)
e	magnitude of electron chare (C)
E	externally applied electric field (V/m)
E_0	by microchannel self-induced electric field (V/m)
k	Boltzmann constant (13.8066×10^{-24} J/K)
l	microchannel length (m)
$n_{i\infty}$	bulk concentration of ions ($1/m^3$)
N_E	dimensionless number, characteristic length ratio
N_κ	dimensionless number, characteristic ratio of electric to hydraulic forces
p	pressure (Pa)
T	temperature (K)
u	velocity component (in the direction of the electric field) (m/s)
z_i	valence of ions i

Greek letters

ε	dielectric constant of the solution
ε_0	permittivity of vacuum (8.854188×10^{-12} F/m)
φ_0	by microchannel self-induced electric potential (V)
γ_0	free surface tension (N/m)
κ^{-1}	Debye length (thickness of the electrical double layer, EDL) (m)
μ	dynamic viscosity (Pa s)
μ_{eo}	electro-osmotic mobility (m^2/V/s), ration of velocity to driving electric field
ρ	solution density (g/l)

example it is proposed to replace a millilitre sample in the 7 ml vial with a microlitre sample in a microchannel of 300 μm width and 18 mm length, which is then analysed by spectrophotometry. Obviously the relevant volume reduction with a factor 6321 by replacing the 7 ml size with 0.62 μl size, implies an almost proportional dose reduction with a factor 6000 at 1 m distance, as proven by Janssens-Maenhout et al. (2007). More information on the Monte Carlo simulations for this proof is given by Buyst (2005). The reduced radiation has several advantages. A direct analysis on the real solution can take place without the need for dilution: This fastens and simplifies the analytical analysis procedure; and the direct results allow an interpretation with a smaller uncertainty range. The analysis can take place in a glove box, no hot cell is needed any longer. The reduction in shielding allows to make the analytical device transportable. The radioactive waste is also reduced, not only because of the volume of the microchip itself but mainly because of the omission of the sample preparation. This means that the analysis is non-destructive and that the sample solution can be re-introduced into the process cycle.

2. The MEMS design

The design of the microchip results as a compromise between the requirements for manufacturing and those for the special treatment of the radioactive solutions. The MEMS of the microchip has to allow reproducible spectrophotometric measurements along the microchannel, in which an electrophoretic flow of the radioactive solution is established. The photospectrometric aspects have been investigated by Nucifora (2004), the micro-fluidic aspects by Macerata (2004) and Matthews (2005) and the thermodynamic by Uyttenhove (2005).

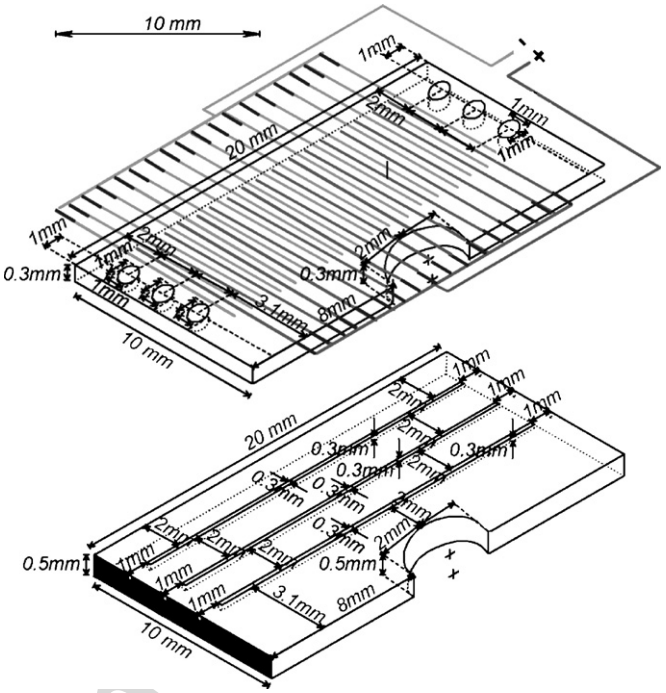

Fig. 1. MEMS design with three microchannels for densitometric and spectrophotometric analysis of radioactive solutions. The gray grid represents the pairs of electrodes (composed of one left and the closest subsequent electrode right), through which a voltage over each pair is imposed in alternating mode by subsequent activation of one left and one right connection.

As shown in Fig. 1 the MEMS base (20 mm × 10 mm × 0.5 mm size) consists of three microchannels, all with 300 μm × 300 μm cross section. The half channel width $a = 150$ μm was chosen as reference length for the fluiddynamic calculations, and the length of each channel $l = 18$ mm can be expressed as $120a$.

The first channel contains the reference solution, the middle one is the optical positioning channel and the third represents the chemical analysis channel, through which the subject radioactive solution is pumped based on the principle of electrophoresis. In a cover, inlets and outlets are foreseen and between the two layers a series of electrodes are inserted to create an electric field along the microchannel length axis. The complete MEMS is embedded in a positioning frame. As will be shown in Section 5, no cooling Peltier element is necessary to keep the temperature variations smaller than 0.5 °C.

As substrate material a high density polyethylene (HDPE) has been selected because this polymer is (i) resistant to acidity and irradiation during the measurement time of maximum 1 day, (ii) transparent for the photospectrometric analysing technique, and (iii) compatible with the material requirements for hot embossing. A first prototype and the mould are made of Si-compounds.

3. Experimental proof of the photospectrometric analysis

3.1. The neodymium reference data

The radioactive solution focussed on in this paper is the spent fuel solution, or so-called input solution as collected in the input accountancy tank of a reprocessing plant. Characterisation of the input solution is the important starting element because no direct measurements of the U and Pu content, the U enrichment and the Pu vector are made on unloaded reactor fuel. This input solution is typically prepared with 3 M nitric acid and the dissolved spent fuel, which contains typically 2 up to 250 g actinide nitrate.

According to Seaborg et al. (1994) the Actinides show a Lanthanide-like behaviour, except that Lanthanides are much less radiotoxic. Lanthanides, such as neodymium (Nd) are chemically characterised by a homogeneous behaviour in aqueous solutions because they form similar chemical compounds with trivalent ions. A non-radioactive, stable surrogate solution of 3 M nitric acid with neodymium, $Nd(NO_3)_3 \cdot 6H_2O$, showed representative absorption peaks in the interesting wavelength region and was therefore selected as reference solution.

A photospectrometric reference data base was setup with the measured absorption peak surface for typical aqueous solutions with different neodymium concentration. As shown in Fig. 2 the by Lambert–Beer required linearity between the Nd concentration and the peak surface at 578 nm, respectively, 740 and 794 nm was obtained with a correlation factor larger than 99.6%. The dependencies of the spectra on the temperature and on the solvent's molarity were examined within the operational conditions range of 15–55 °C temperature variations and of 0.1–8.0 mol/l molarity variation. As an example, the effects on the peak surface at 578 nm are shown in Figs. 3 and 4.

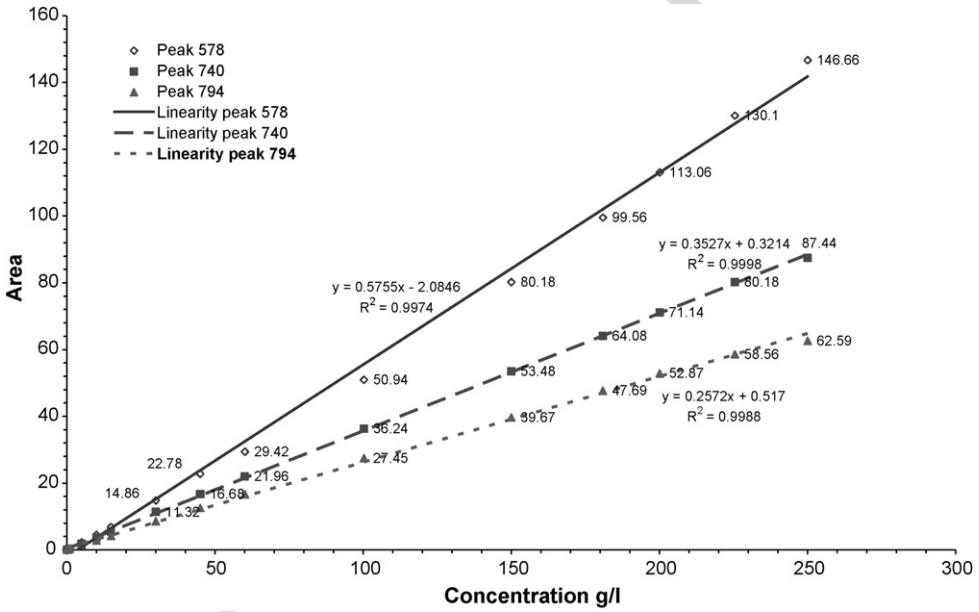

Fig. 2. Linear relation between the Nd concentration and the surface area of the peak at 578 nm, of the peak at 740 nm and of the peak at 794 nm, each calculated on five bins of 2 nm centred around the highest recorded absorbance value.

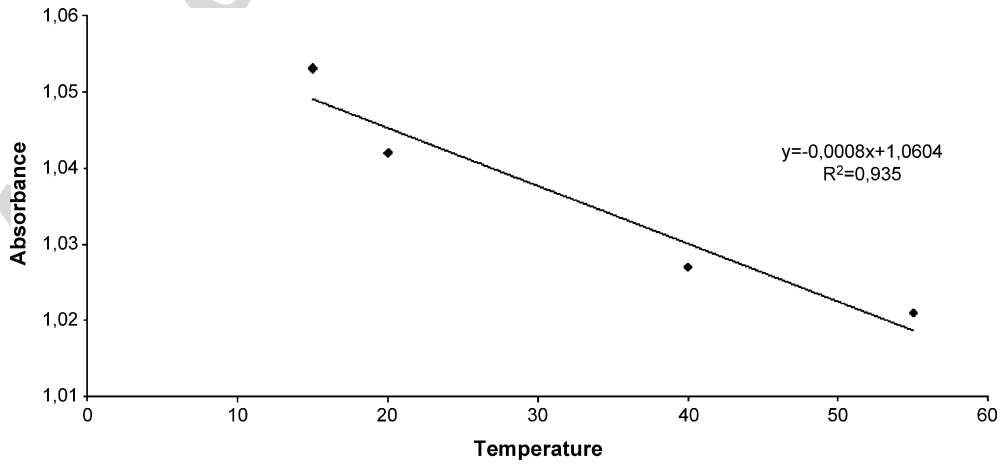

Fig. 3. Influence of the temperature on the absorbance values of the peak at 578 nm, for a 3 M nitric acid solution with 18 g/l Nd.

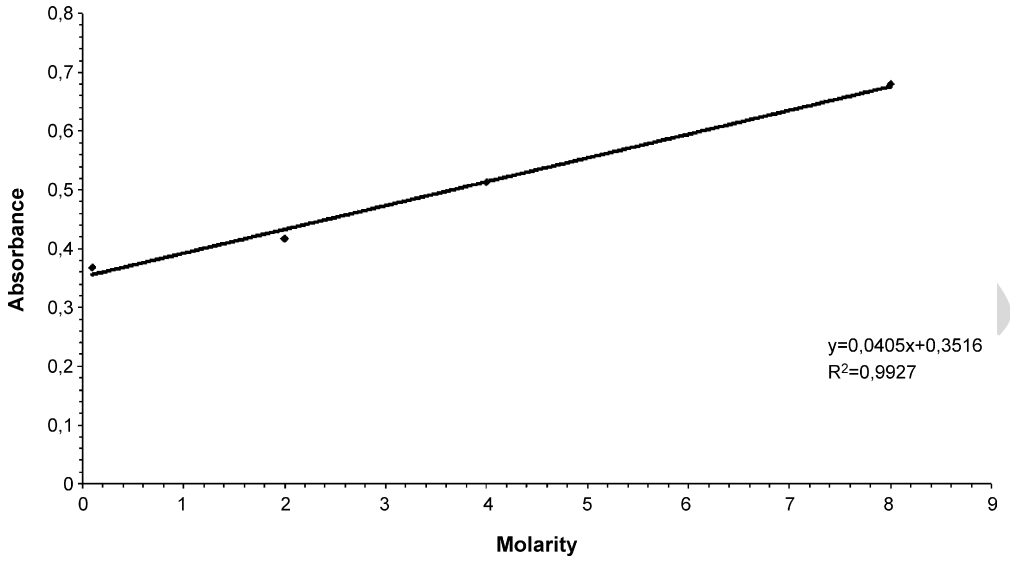

Fig. 4. Influence of the molarity of the nitric acid solution with 8.5 g/l Nd at 20 °C on the absorbance value of the peak at 578 nm.

The temperature effects can be explained as a superposition of density and thermochromatic effects on the spectra and are negligible—less than 0.06% decrease in absorbance per temperature degree. The variation in molarity leads to a change in extinction coefficient (due to pH and colour change) and a shift in the peak's position to larger wavelength values. The influence of molarity was only checked for one concentration of Nd because the absorbance increased relatively only 3.8% per mole and the nitric acid solutions used in practice are standardly 3 M. The peak at 740 nm was focused on for further feasibility study of the photospectrometric analysis on a microsample because that peak is characterised by the largest width on half maximum in the absorption spectra and the calibration curve showed for the same measurement precision the best linearity (highest correlation factor) in comparison with the peak at 578 nm and at 794 nm.

3.2. Photospectrometric measurements with a microsample

The reproducibility and detection limits of the measured absorption spectra have been examined while downscaling the sample size and the path length. The results of the experimental tests with a microsample in a cell of 62 μl in Fig. 5 have demonstrated the feasibility of photospectrometric concentration measurements in a validity range of 18 till 230 g/l. Given that the absorption spectra for the traditional vial show similar quality with a half width on maximum height of 1 on 20 nm for concentrations up to 0.1 g/l, a reduction (with factor 18) in the lower limit for concentration measurements is present. The Lambert–Beer relationship between the concentration and the surface of the absorption peak at 740 nm showed a linear correlation with a correlation factor larger than 99.9%, as can be noticed in Fig. 6.

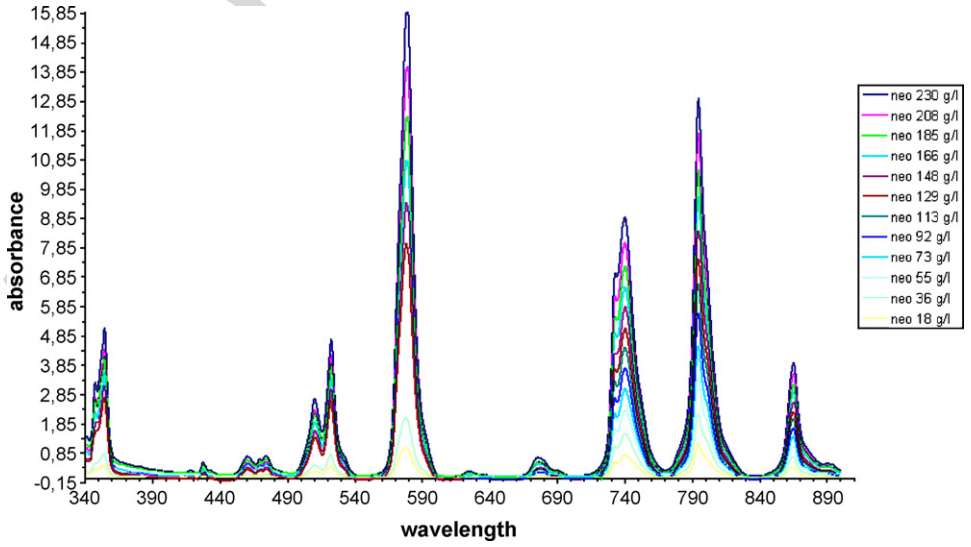

Fig. 5. Absorption spectra for a microsample of 62 μl filled with 3 M nitric acid in which Nd with different concentrations (varied from 230 till 18 g/l) is solved.

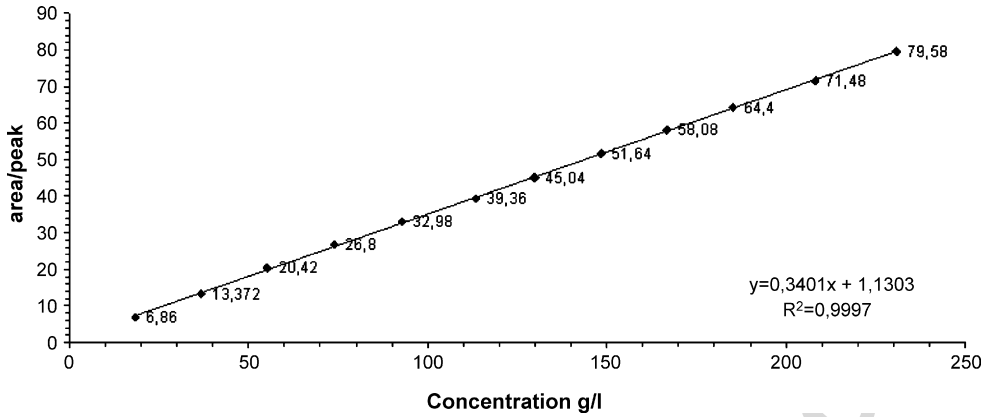

Fig. 6. Photospectrometric measurements with the microsample of 62 ml shows the Lambert–Beer linearity between the Nd concentration and the surface area of the peak at 740 nm, calculated on five bins of 2 nm centred around the highest recorded absorbance value.

The path length along which the light is absorbed, influences directly the measurable range of concentrations. For a concentration of 55 g/l is a path length of 10 mm leading to saturation of the measurement, whereas a path length of 1 mm gives good results and a path length of 0.12 mm is affected by a large uncertainty.

To anticipate problems with the real radioactive solutions, similar photospectrometric analyses with real target solutions $UO_2(NO_3)_2$ and $PuO_2(NO_3)_2$ in 3 M nitric acid were successfully carried out. The potential presence of microparticles in the solution (for 0.1 till 1%) was investigated separately by Nucifora (2004). In the case with 0.35 μm silica particles the standard Rayleigh scattering effect in the spectra was observed that could be corrected for. In the case with carbon particle agglomerates of 100 μm diameter, already a presence of 0.035% indicated that the measurement (with 2.5% error) overestimates the absorbance values.

4. The fluid flow of the radioactive solution

4.1. Fluid properties

To evaluate the fluid flow it is needed to know the density and viscosity of the radioactive solution in function of the actinide concentration. The subject input solution, a 3 M nitric acid in which spent fuel is dissolved leading to 2 up to 250 g actinide nitrate, can be well-represented with regard to the density and viscosity by the 3 M nitric acid with Nd reference solution. Its physical properties in function of the Nd concentration at varying temperatures and acidities of the solution are determined experimentally.

The density varies linearly with the concentration as given by the relations of Tanaka and Hosoma (2003). Therefore, we can characterise the typical input solutions by a reference density of 1.4 g/cm^3 with 150 g/l U in the 3 M nitric acid and at 25 °C and by a reference viscosity of 1.9 mPa s with 150 g/l U in the 3 M nitric acid at 25 °C. The physical properties, density ρ and dynamic viscosity $\mu = \rho \cdot \nu$, measured with a precision of ±1 g/l, respectively ±1 μPa s, have been tabulated for a reference solution of 3 M nitric acid with different Nd concentrations in function of the temperature in Table 1.

4.2. Capillary flow

The flow in microchannels differs strongly from the classical one in macrochannels, as described by Gad-el-Hak (1999) amongst others. Based on the electrical double layer (EDL) theory, presented a.o. by Israelachvili (1998), we assume that the boundary layer of the liquid is composed of a nanolayer and

Table 1
Physical properties of the 3 M nitric acid solution with different Nd concentrations (determined with a precision of ±0.5%), density ρ and dynamic viscosity $\mu = \rho \cdot \nu$, measured with a precision of ±1 g/l respectively ±1 μPa s for different temperatures (determined with a precision of ±0.2 °C)

Nd concentration (g/l)	T = 15 °C		T = 20 °C		T = 25 °C		T = 35 °C		T = 45 °C	
	ρ (g/l)	μ (μPa s)	ρ (g/l)	μ (μPa s)	ρ (g/l)	μ (μPa s)	ρ (g/l)	μ (μPa s)	ρ (g/l)	μ (μPa s)
249.48 ± 0.5%	15,409	4666.0	1535.9	4045.5	1531.1	3542.1	1521.9	2778.3	1512.2	2250.3
199.93 ± 0.5%	14,568	3360.3	1451.5	2945.0	1447.5	2602.3	1438.8	2087.4	1429.1	1714.2
150.06 ± 0.5%	13,700	2493.0	1366.2	2206.5	1361.9	1966.4	1354.1	1599.2	1345.4	1327.4
124.91 ± 0.5%	13,233	2158.4	1319.1	1919.1	1315.5	1722.5	1307.9	1402.0	1299.7	1174.7
100.12 ± 0.5%	12,779	1893.2	1274.1	1681.8	1270.8	1514.8	1263.4	1243.8	1255.8	1043.6
74.99 ± 0.5%	12,308	1659.6	1227.0	1477.9	1224.0	1328.5	1217.1	1097.1	1210.2	925.4
49.99 ± 0.5%	11,858	1489.5	1182.5	1332.5	1179.3	1201.4	1173.3	992.8	1166.3	840.3
25.04 ± 0.5%	11,442	1351.5	1141.0	1210.5	1138.0	1091.1	1132.1	906.9	1125.8	767.1
10.01 ± 0.5%	11,193	1278.2	1115.8	1144.4	1113.0	1030.4	1107.1	859.4	1101.2	731.4
1.99 ± 0.5%	11,047	12451.3	1102.8	1115.4	1099.4	1006.4	1093.9	838.3	1087.6	709.1
0	11,023	1232.9	1098.9	1109.4	1096.1	997.6	1090.5	831.2	1084.3	705.9

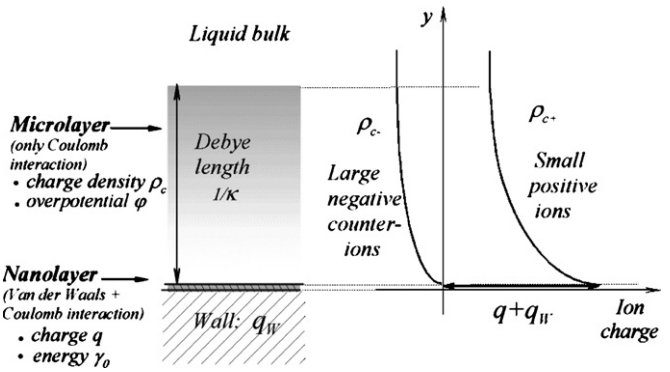

Fig. 7. Microscopic model of liquid/solid interface.

a microlayer, as shown in Fig. 7. The nanolayer includes all molecular effects and is for simplicity modelled by an infinitely thin layer with a surface energy density γ_0 and with a surface charge density q. This surface charge density causes a long-range Coulomb effect as described in the EDL theory with a concentration of ions in the microlayer, and thus with an electric energy in it.

The surface energy of the microlayer becomes significantly larger than the one of the nanolayer in the case of a liquid interface in contact with a solid wall, as observed by Young (1805). Under the assumption that the wall is completely inert, a wall surface charge q_W induces an ion concentration in the microlayer with an additional electric energy.

To estimate the thickness of the microlayer for the solution with a bulk concentration $n_{i\infty}$ of ions (valence z_i) at temperature T, the Debye length has been calculated for different salt concentrations with Eq. (1):

$$\kappa^{-1} = \left(\frac{\sum z_i^2 e^2 n_{i\infty}}{\varepsilon \varepsilon_0 k T} \right)^{-1/2} \quad (1)$$

and herewith also the (dimensionless) number

$$N_\kappa = \kappa \cdot a \quad (2)$$

Thereby the dielectric constant ε has been derived with the relationships of Wang and Anderko (2001). The Debye length varies linearly from 0.9 nm for a 3 M nitric acid with 2 g/l lanthanide to 0.07 nm for a 3 M nitric acid with 200 g/l lanthanide, which is in agreement with Atkin's data (2004).

The EDL-layer yields a self-induced EDL-potential φ_0 which fulfils the Poisson-Boltzmann equation and a microlayer at the wall boundary with a charge density gradient, as described in detail by Janssens-Maenhout and Schulenberg (2003). The calculated Debye length in nm range allows to model the EDL with vanishing thickness but with a given surface charge density, that differs from the bulk charge density.

This means that the microchannel flow can be calculated as a macroscopic laminar flow but with a slip condition at the boundary, simulating the EDL. The slip velocity is calculated in function of the self-induced electric field E_0 ($=-\nabla\varphi_0 = -\Delta\varphi_0/\Delta\kappa^{-1}$) and the pressure drop $\Delta p/l$ via the

Table 2
Fluiddynamic characteristic parameters of typical $Nd(NO_3)_3{\cdot}6H_2O$ solutions through the microchannel and the dimensionless numbers: (i) ratio of Debye length to half microchannel width N_κ; (ii) and ratio of electric to hydraulic forces N_E (The liquid properties, which have not been measured and recorded in Table 1, are taken from Landolt-Börnstein (1956))

Concentration of NO_3^- (mol/l)	Concentration of Nd (g/l)	Debye length $1/\kappa$ ($T=25\,^\circ$C) (nm)	Charge, q ($T=25\,^\circ$C) (C/m^2)	Dielectr. cst. ε ($T=25\,^\circ$C)	EDL potential φ_0 (mV)	Free surface tension γ_0 (N/m)	Pressure drop Δp_{tot} (Pa)	N_κ	N_E
1.00E−07	1.00E−07	967.26	0.058000	80	543.78	0.072984	150.00	155.08	4.324E−03
0.042	2	1.68	0.016203	50	243.98	0.069851	140.33	89534.44	3.592E−06
0.21	10	1.65	0.016907	49	244.30	0.070368	138.11	90790.83	3.604E−06
0.52	25	1.59	0.016837	46	245.63	0.071610	134.34	94217.80	3.589E−06
1.04	50	1.56	0.017100	44	246.90	0.073364	127.02	96078.88	3.742E−06
2.07	100	1.51	0.016978	40	250.16	0.077235	111.32	99114.01	4.194E−06
2.59	125	1.48	0.017614	37	253.05	0.079704	103.31	101252.67	4.475E−06
3.11	150	1.47	0.017366	35	255.32	0.081985	94.34	102362.74	4.890E−06
4.15	200	1.49	0.017385	33	259.05	0.086342	74.21	100902.57	6.399E−06
5.18	250	1.49	0.018219	30	263.87	0.090961	51.65	100968.34	9.358E−06

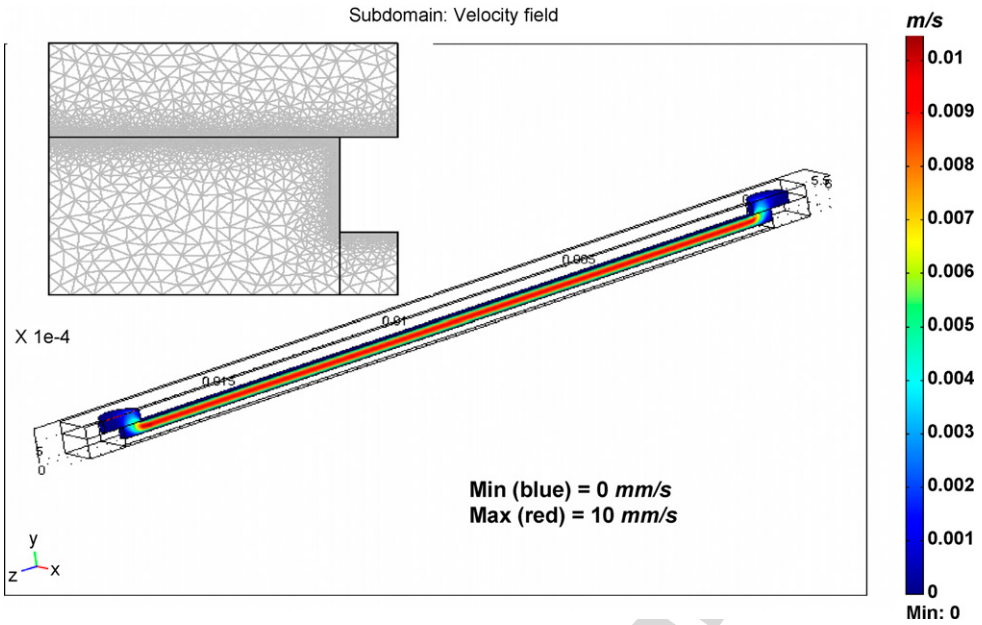

Fig. 8. Microchannel flow simulation with the finite element code FEMLAB.

use of the following characteristic number (dimensionless)

$$N_E = \frac{8zen_{\infty i}l}{(\kappa a)^2}\frac{E_0}{\Delta p} \tag{3}$$

that expresses the ratio of electric forces to hydraulic forces in the microlayer. Typical parameters for solutions of various acidity, embedded in a glass substrate are given in Table 2. For acid solutions, the number N_E is three orders of magnitude lower than for non-acid aqueous solutions. Therefore, the self-induced electric field E_0 can be neglected for the commonly used solutions of 3 M nitric acid in the subject microchip.

The laminar flow in the microchannel will show a normal Poiseuille profile in case of no external electric field. For an electrophoretic filling of the microchannel an external electric field is applied, which will cause a slip at the wall. In aqueous, bipolar solutions a negative effect might be expected in the boundary layer with ions of opposite sign compared to the ions in the bulk solution. Numerical simulations have been carried out to identify potential death zones even in the case of a negative slip condition at the microchannel wall[1]. The laminar flow in the microchannel has been simulated assuming symmetry at the central vertical plane of the horizontal microchannel and optimising the grid with a 3D hybrid mesh of which cross section is given in Fig. 8. As driving force $\Delta p = 50$ Pa was specified over the inlet/outlet boundary and at the wall a slip condition was imposed with a horizontal velocity of -1.1 mm/s, set to 20% of the maximum velocity.

The flow was fully developed at 150 μm from the inlet. The horizontal velocity over the microchannel cross section at 150 μm from the inlet, as shown in Fig. 9, shows a Poiseuille profile of the laminar flow shifted down with 20% corresponding to the slip condition. No death zones have been indicated by the simulation for the filling of the microchannel (with and without slip). Therefore, it can be assumed that concentration profiles averaged over the cross section are representative.

4.3. Filling of the microchannel

Taking advantage of the capillary effects of the microchannel flow, the technique of filling by means of electrophoresis has been selected because it was the most suitable method to move the radioactive liquid. Other possibilities, by means of micro-pumps or by the surface acoustic wave principle have been evaluated as not appropriate. Movement with mechanical parts is always avoided in radioactive environments. Moreover,

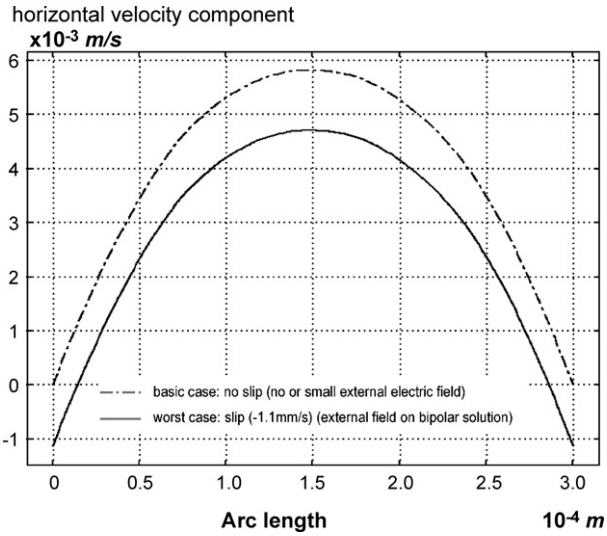

Fig. 9. Results of the simulated microchannel flow: (i) case of no external electric field: Poiseuille profile over the flow cross-section; (ii) case of external field on bipolar solution: velocity profile after 150 μm from inlet.

[1] No slip condition has been applied in the inlet and outlet regions.

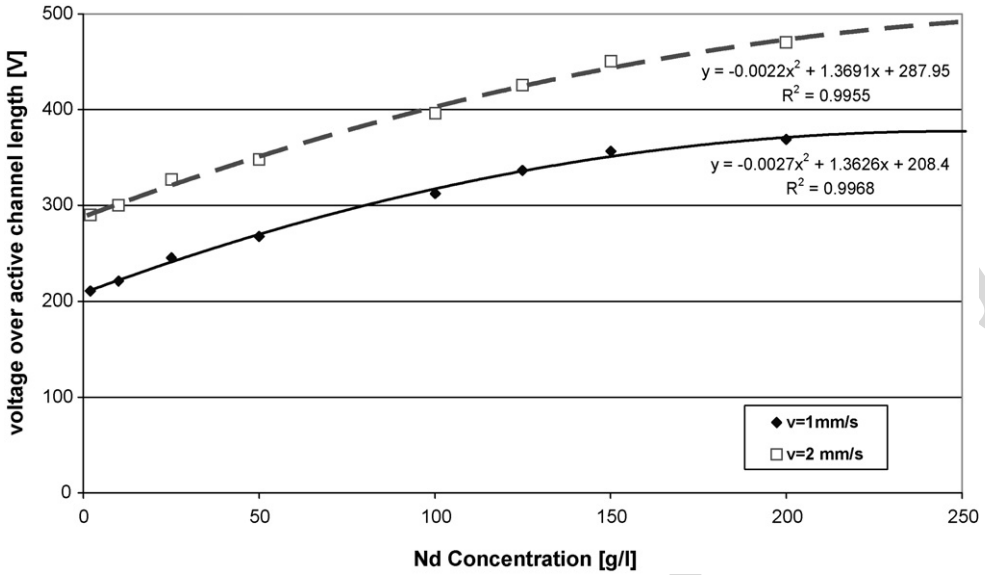

Fig. 10. Externally applied electric field forces the liquid into the microchannel.

the liquid from the input accountancy tank may contain micro-size particles. As the liquid can be considered as a homogeneous emulsion, the properties, density, viscosity and surface tension remain valid. However due to the presence of particles the sound acoustic wave principle could not be applied for moving the liquid while determining the density.

The fluid will not be moved into the microchannel with a smooth constant flow but an electrophoretic peristaltic flow will be induced by a series of electrodes with constant potential difference and alternatively becoming active. With all the liquid properties of the radioactive solution, the pressure drop was calculated by superposition of the dynamic and static pressure drop. The latter is dominated by the capillary pressure, resulting from the adhesion and surface tension.

To fill the microchannel by electrophoresis, an external axial electric field has to be applied such that the electric forces counteract the pressure forces. These electric forces increase with increasing salt concentration because of the growing hydrostatic and dynamic pressure drop for higher density liquids and because of the diminishing capillary action. The flow in the microchannel has been numerically simulated with FEMLAB, using an external electric field on the ionic solution as driving force. The liquid movement into the channel can be expressed in relation to the required electric field by means of the electro-osmotic mobility

$$\mu_{\mathrm{eo}|150\,\mathrm{g/l\,Nd}} = \frac{u}{E} = \frac{1\,\mathrm{mm/s}}{19.8\,\mathrm{V/mm}} = 0.05\,\mathrm{mm^2/V/s} \qquad (4)$$

This means that to fill the microchannel with a reference solution of 150 g/l Nd an electric potential of 356 V is to be applied over the total active microchannel length of 18 mm in order to have a mean velocity of 1 mm/s. The major part of the electric forces (73%) compensate for the capillary force, the remaining part 27% for the dynamic pressure loss. For a mean velocity of 2 mm/s an electric potential of 451 V is needed. Fig. 10 represents the total electric potential, necessary to move the liquid in the microchannel with mean velocities of 1 and 2 mm/s. In practice the electric potential will be established by inserting 10 micro-electrodes with a potential difference of 50 V. This 50 V potential difference is applied between succeeding electrodes in an alternating way from the first two till the 9th and 10th. The alternation of voltage between succeeding electrode pairs will cause a suction of the liquid in the microchannel in a peristaltic way.

The electrophoretic flow was simulated with finite elements for the case of an external potential of 356 V over the 18 mm flow length to drive a 3 M nitric acid solution with 150 g/l Nd. Fig. 11 shows the resulting Poiseuille profile of the developed flow (150 μm from the inlet), now shifted up towards values between 1.434 and 1.438 mm/s.

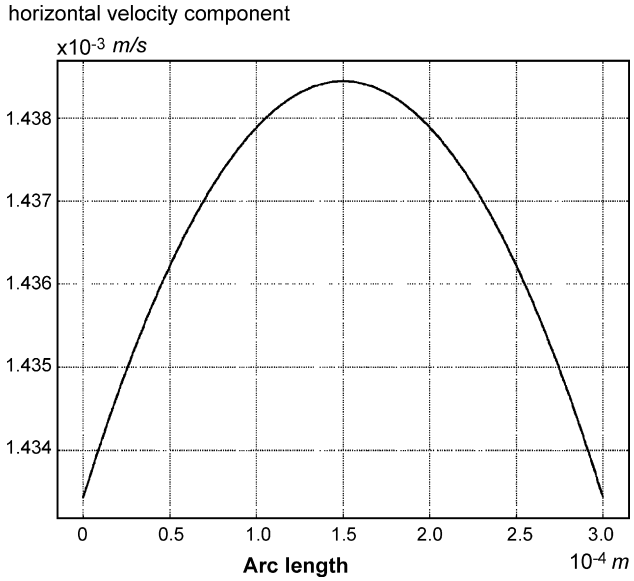

Fig. 11. Simulated cross section profile of the electrophoretic flow: the typical Poiseuille profile for the microchannel flow is again observed, shifted towards higher velocities because of the driving electrical field.

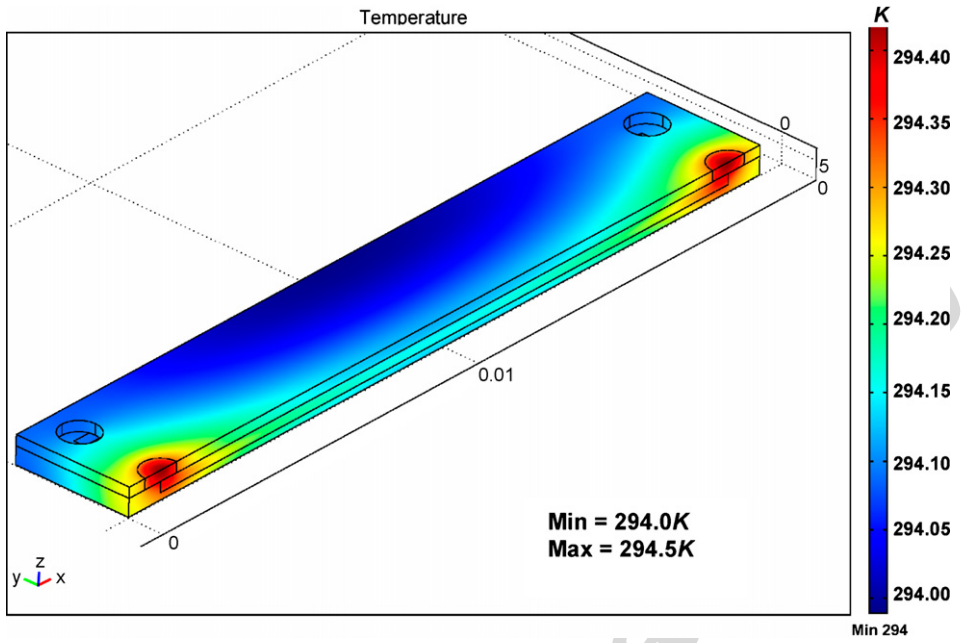

Fig. 12. COMSOL simulation of the temperature distribution for a heat source in the microchannel of 1.5 mW, showing a maximum difference of 0.5 °C and the inlet and outlet channel, which are the hot spots because of their relative large volume. The microchip thermal behaviour was simulated with a heat transfer coefficient for the upper cover of 12.3 W/m/K, and 10.9 W/m/K at the bottom. The side of the HDPE substrate showed a heat transfer coefficient of 6.0 W/m/K.

5. Thermo-dynamic behaviour of the filled microchannel

5.1. Heat transfer from the microchannel to the ambient

It was needed to analyse as well the thermo-dynamic effects of the microchannel, because it will be filled with a radioactive and therefore hot solution. For these analyses the radioactive fluid can be considered as a thin heat source, which consists in the specific heat of the hot solution with the decay heat. Only a heat source in the order of milliWatt needs to be taken into account because of the microvolume that contains this specific heat. The heat transfer from the hot microchannel fluid towards the ambient was modelled with conduction over the microchip material and with free convection at the outer chip wall. For a heat source of 50 mW a maximum temperature difference of 5 °C was obtained between the initial and final temperature of the microchip with a steeper temperature gradient above the horizontal microchip because of the natural convection effect.

For a more realistic case of 1.5 mW heat source the temperature distribution after thermodynamic equilibrium is shown in the simulation of Fig. 12 and reached a maximum temperature difference of 0.5 °C. This range of temperature difference was confirmed with a finite volume simulation for a 1.0 mW heat

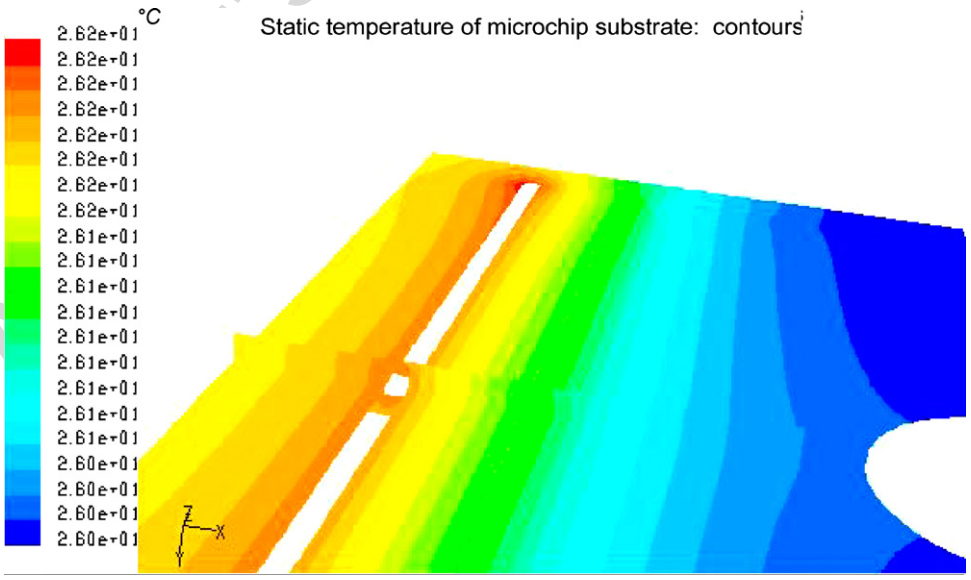

Fig. 13. FLUENT simulation of the temperature distribution in the microchip for a heat source of 1 mW.

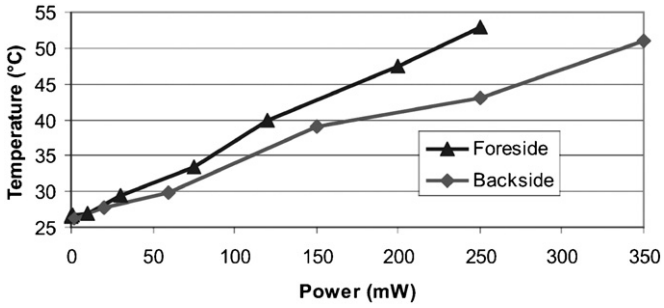

Fig. 14. Average temperature measured at the surface of the microchip (in which a copper wire is inserted to simulate the radioactive solution heat source) by a thermographical camera for increasing power at the foreside and at the backside.

source, in which the temperature difference dropped down to 0.2 °C, as shown in Fig. 13.

In order to validate the thermodynamic simulation model of the microchip it is needed to compare with real experiments. Uyttenhove (2005) carried out a thermographical experiment, in which the heat source of the radioactive solution was simulated with a copper wire in the microchannel. For increasing power, the surface of the upper cover and substrate bottom has been registered with a thermographical camera and the results of Fig. 14 have been found.

The experimental results indicate that below 1 mW no temperature difference over the chip larger than 0.5° can be measured. The simulations are in agreement with this observation. A somewhat larger calculated temperature difference than measured can be accepted because the measured temperature distribution might be perturbed by a potential air layer between the copper wire and the microchannel.

It could definitely be concluded that the thermodynamic simulations are modelling the real microchip within acceptable variation range. Moreover, it could be concluded for the microchip that a Peltier element for cooling the microchip is not needed, given the very low heat source.

5.2. Thermal stresses in the microchip

Finally it is important to analyse of the microchip undergoes deformation due to temperature changes in the microchannel. A deformation would perturb the absorptiometry substantially because the light needs to transverse the complete channel length. A deformation of the channel itself or in relation to the positioning channel could make the absorptiometry results invalid. Moreover, the dependence of the absorption peaks on the wavelength is sensitive to the temperature. A change in temperature could induce a shift of the absorption peaks towards other wavelengths.

With finite elements for a heat flux of 60 mW/cm^2 (corresponding to the case of 1.5 mW heat source) the temperature distribution in the microchip and the distribution of the stresses were calculated. For the first microchip in Si compounds with Silicon substrate and Pyrex cover a maximum tensile stress of 48 MPa and a maximum compressive stress of 110 MPa was obtained. For the microchip with HDPE substrate and glass cover, Fig. 15 shows that the von Mises stresses vary from 1 to 25 MPa.

The von Mises stresses of 20 MPa on the HDPE substrate have to be compared with the maximum yield stresses for the HDPE (plastic) of 28 MPa. It could be concluded that the stresses are acceptable, even without water bath or cooling element (Peltier). However it is recommended to utilise materials with similar expansion coefficients. Large stresses are observed between the

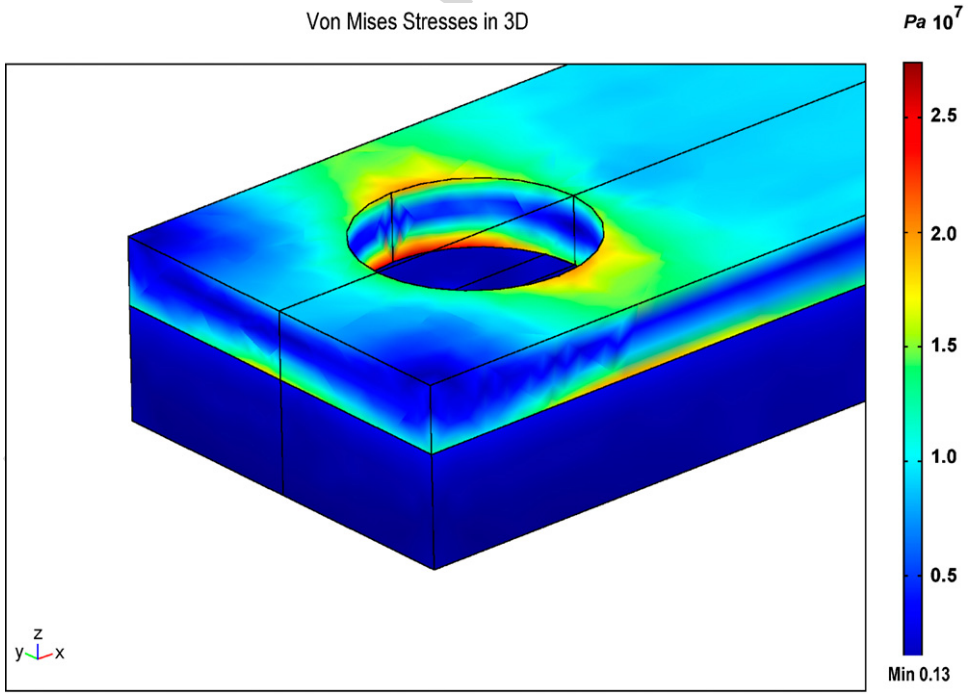

Fig. 15. Von Mises stresses in 3D in the microchip with a high density polyethylene (HDPE) substrate and glass cover, and filled with a radioactive solution represented by a heat source of 1.5 MW/m^3.

Pyrex cover and silicon substrate because of strongly different volumetric expansion.

6. Conclusions

This research work reports on the feasibility to apply a microchip for the chemical analysis of a radioactive solution for nuclear safeguards purposes. Firstly, the validity of the concentration measurements by photospectrometry of the wave-length specific light absorption peaks was focused at. Then the microfluiddynamic behaviour was analysed to develop a real suction of the radioactive solution in the microchannel by electrophoresis. Finally the thermodynamic aspects were addressed to guarantee the stability and reproducibility of the microchannel measurement results.

The photospectrometric experiments have proven that:

- The measurements results are reproducible and reliable, showing the Lambert–Beer linearity, for aqueous solutions with a concentration in the range of 18 till 230 g/l salt. To avoid systematic uncertainties a photospectrometric reference data base has been setup for a representative aqueous solution of 3 M nitric acid with Nd in different concentrations, varying from 0 till 250 g/l.
- The path-length has to be selected in function of the ion concentration in the radioactive solution: 1 mm for solutions with concentrations in the range of 50 g/l salt in the aqueous solution, 0.1 mm for solutions with concentrations of 250 g/l and 10 mm for solutions with 5 g/l salt.

The micro-fluiddynamic simulations demonstrated that:

- The radioactive solution can be sucked into the microchannel by means of electrophoresis with an external field of 356 V/18 mm.
- The microchannel flow is laminar and shows a typical Poiseuille profile shifted down because of the slip boundary condition that is needed to model the electrophoretic microchannel flow.
- The average over the cross-section is representative for the entire solution because no death zones would be noticed.
- The flow is fully developed after 150 μm from the inlet. Therefore, the flow can be assumed to be homogenous of the complete flow path along the axis of the microchannel.

The thermo-dynamic investigations demonstrated:

- The thermo-dynamic model can be accepted as valid to predict the temperature distribution in similar microchip designs, since the simulations were successfully validated with the experimental results.
- The microchannel with radioactive hot solution can be considered as almost isothermal because of the very low specific heat with decay heat of the radioactive solution.
- The thermal stresses observed in the microchip are acceptable in comparison to the yield stresses of the material. No special cooling with water bath or Peltier cooling element is necessary. The deformation will not perturb significantly the absorptiometry results.

Acknowledgements

The authors are grateful to their student-colleagues, J. Buyst, E. Macerata, R. Matthews and W. Uyttenhove who contributed to this subject for their master thesis, as well as to the additional promotors, J. Howell of Glasgow University and M. Mariani of the Politecnico di Milano. Also a word of thanks to C.F. Pirri and S. Guastella of the Material & Microsystems Laboratory at the Politecnico di Torino for the fabrication of a prototype microchip.

References

Atkins, P.W., 2004. Chimica Fisica. John Wiley & Sons (Chapter XI).
Buyst J., 2005. Nuclear safeguards by lab on the microchip: deterministic calculation of radioactive dose reduction by volume size reduction. Thesis for the Engineering Degree at the University Ghent, June.
Gad-el-Hak, M., 1999. The fluid mechanics of microdevices—the Freeman scholar lecture. J. Fluids Eng. 121, 5.
Israelachvili, J.N., 1998. Intermolecular and Surface Forces, second ed. Academic Press, San Diego.
Janssens-Maenhout, G., Schulenberg, T., 2003. An alternative description of the interfacial energy of a liquid in contact with a solid. J. Colloid Interface Sci. 257, 141–153.
Janssens-Maenhout, G., Buyst, J., Peerani, P., 2007. Reducing the radioactive doses of liquid samples taken from reprocessing plant vessels by volume reduction. J. Nucl. Eng. Design 237, 880–886.
Landolt-Börnstein, 1956. Zahlenwerte und Funktionen aus Physik, chemie, Astronomie, Goephysik und Technik, vol. 2., sixth ed. Springer Verlag, Berlin.
Macerata, E., 2004. Micro-fluiddynamic constraints for the lab on the microchip to analyse radioactive solutions, tesi di laurea, Politecnico di Milano, Nucl. Eng. Dep., June.
Nucifora, S., 2004. Nuclear safegurards by lab on the microchip: spectrophotometric tests of radioactive solution on microsample, tesi di laurea, Politecnico di Milano, Nucl. Eng. Dep., April.
Matthews, R.M., 2005. Thermo-fluid-dynamic evaluation of a micro-electro-mechanical device for the analysis of radioactive solutions. Master Thesis for Control Engineering. University of Glasgow, June.
Seaborg, G., Gscheider Jr., K.A., Eyring, L., Chopping, G.R., Lander, G.H., 1994. Handbook on the Physics and Chemistry of Rare Earths: Lanthanides/Actinides Chemistry, vol. 18. Elsevier Science, Amsterdam.
Tanaka, H., Hosoma, T., 2003. Comparison of density equations for plutonium–uranyl–nitric solution in a tank and its application to find unexpected error sources. In: Proceedings of the ESARDA Annual Meeting, Stockholm, May.
Uyttenhove W., 2005. Thermodynamic evaluation of a microchip to analyse radioactive solutions. Thesis for the Nuclear Engineering Degree at the BNEN. University Ghent, September.
Wang, P., Anderko, A., 2001. Computation of dielectric constants of solvent mixtures and electrolyte solutions. Fluid Phase Equilib. 186, 103–122.
Young, T., 1805. An essay on the cohesion of fluids. Philos. Trans. R. Soc. 95, 65.